



VICTORIA UNIVERSITY
MELBOURNE AUSTRALIA

Least square support vector and multi-linear regression for statistically downscaling general circulation model outputs to catchment streamflows

This is the Published version of the following publication

Dhanapala Arachchige, Sachindra, Huang, Fuchun, Barton, Andrew and Perera, B. J. C (2013) Least square support vector and multi-linear regression for statistically downscaling general circulation model outputs to catchment streamflows. *International Journal of Climatology*, 33 (5). pp. 1087-1106. ISSN 0899-8418,(print), 1097-0088 (online)

The publisher's official version can be found at
<http://onlinelibrary.wiley.com/doi/10.1002/joc.3493/pdf>
Note that access to this version may require subscription.

Downloaded from VU Research Repository <https://vuir.vu.edu.au/21966/>

Least square support vector and multi-linear regression for statistically downscaling general circulation model outputs to catchment streamflows

D. A. Sachindra,^{a*} F. Huang,^a A. Barton^{a,b} and B. J. C. Perera^a

^a Victoria University, Melbourne, Victoria, Australia

^b Grampians Wimmera Mallee Water Corporation, Horsham, Victoria, Australia

ABSTRACT: This study employed least square support vector machine regression (LS-SVM-R) and multi-linear regression (MLR) for statistically downscaling monthly general circulation model (GCM) outputs directly to monthly catchment streamflows. The scope of the study was limited to calibration and validation of the downscaling models. The methodology was demonstrated by its application to a streamflow site in the Grampian water supply system in northwestern Victoria, Australia. Probable predictors for the study were selected from the National Center for Environmental Prediction/National Center for Atmospheric Research (NCEP/NCAR) reanalysis data set based on the past literature and hydrology. Probable variables that displayed the best significant correlations, consistently with the streamflows over the entire period of the study (1950–2010) and under three 20-year time slices (1950–1969, 1970–1989 and 1990–2010) were selected as potential predictors. To better capture seasonal variations of streamflows, downscaling models were developed for each calendar month. The standardized potential predictors were introduced to the LS-SVM-R and MLR models, starting from the best correlated three and then, others one by one, based on their correlations with the streamflows, until the model performance in validation was maximized. This stepwise model development enabled the identification of the optimum number of potential variables for each month. The model calibration was performed over the period 1950–1989 and validation was done for 1990–2010. LS-SVM-R model parameter optimization was achieved using simplex algorithm and leave-one-out cross-validation. The MLR models were optimized by minimizing the sum of squared errors. In both modelling techniques, validation was performed as an independent simulation. In calibration, LS-SVM-R and MLR models displayed equally good performances with a trend of under-predicting high flows. During validation, LS-SVM-R outperformed MLR, though both techniques over-predicted most of the streamflows. It was concluded that LS-SVM-R is a better technique for statistically downscaling GCM outputs to streamflows than MLR, but still MLR is a potential technique for the same task. Copyright © 2012 Royal Meteorological Society

KEY WORDS statistical downscaling; support vector machine; multi-linear regression; streamflow; general circulation models

Received 17 November 2011; Revised 6 March 2012; Accepted 25 March 2012

1. Introduction

Climate change due to increasing greenhouse gas (GHG) concentrations in the atmosphere is a major concern in today's world (Hughes, 2003). Scientific details on climate change and its impacts began to reveal in 1980s (Muzik, 2002). Today, it is clearly understood that climate change is affecting the physical and biological systems in the Earth, and it is expected to continue its impacts in the future (Sullivan and Huntingford, 2009). Human activities, including the combustion of fossil fuels and changes in land cover such as deforestation and agricultural practices, have led to increased atmospheric GHG concentrations, which change the global energy balance causing turmoil in climate (Xu *et al.*, 2009). Although the most clear climate change indicator is the

rising surface air temperature, changes in precipitation imposes more impacts on humans as well as flora and fauna (Benestad *et al.*, 2007). Climate change sheds its impacts on plant physiology, productivity and growth, since photosynthesis, which is responsible for the above-mentioned processes of plants, is directly influenced by the atmospheric carbon dioxide (leading GHG) concentration and temperature (Hughes, 2000). Furthermore, over the past few decades, changing climate has modified the distribution and existence of certain species of animals around the world (Root *et al.*, 2003). Climate change alters the flows in streams, river water quality and ecology of freshwater resources (Whitehead *et al.*, 2009).

Proper management of water resources requires the accurate knowledge of runoff (or streamflow), and seasonal and annual behaviours of the streamflow, under changing climate (Phillips *et al.*, 2003). According to Ruiz *et al.* (2007), a reliable forecast of streamflow will help the control of surface runoff and allocation of water

* Correspondence to: D. A. Sachindra, School of Engineering and Science, Footscray Park Campus, Victoria University, P.O. Box 14428, Melbourne, Victoria 8001, Australia.
E-mail: sachindra.dhanapalaarachchige@live.vu.edu.au

for domestic and industrial needs, irrigation, and environmental flows. The ever rising demand and possible changes in the way water resources are distributed in future will be a challenge for water resources managers around the world (Chiew *et al.*, 2010). During 1997–2008, the average rainfall over the southern part of southeast Australia dropped by about 11% from the long-term average causing a decline in runoff of about 35% (Chiew *et al.*, 2010). Since 1997, till heavy rainfalls in late 2010 and early 2011, the Australian state of Victoria was in the grip of a severe drought. In the decade of 1998–2007, the annual average rainfall over Victoria decreased by about 13% from the long-term average and the highest decline in Victorian rainfall, which was about 28% occurred in the autumn (Victorian Government Department of Sustainability and Environment, 2008). During this drought, the Melbourne and the Grampians water supply systems in Victoria experienced inflow drops of 38% and 75%, respectively, from the long-term average. Considering the consequences of such droughts, the prediction of future streamflows under changing climate is a timely need.

General circulation models (GCMs) are regarded as the most reliable and advanced tools available to simulate global climate hundreds of years into future (Anandhi *et al.*, 2008; Ghosh and Mujumdar, 2008). Heyen *et al.* (1996) stated that GCMs are powerful tools for the analysis of the global climate. GCMs are widely used to assess the impacts of rising GHG concentrations on the global climate (von Storch *et al.*, 1993). These GCMs produce forecasts of the global climate based on possible future GHG emission scenarios. In a GCM, conservation laws of mass, energy and momentum are applied to the atmosphere along with various assumptions, to simplify the naturally chaotic behaviour of the atmosphere. The spatial resolution of a present day GCM is in the order of a few hundred kilometres (Tripathi *et al.*, 2006). The spatial resolution varies from one GCM to another (Smith and Chandler, 2009). According to von Storch *et al.* (1993), GCMs are capable of simulating the global climate realistically on a coarse scale. However, there is a considerable difference between the grid resolution of present day GCMs and the resolution needed by catchment-level hydroclimatic studies (Maurer and Hidalgo, 2008). Owing to the coarse resolution, the direct use of GCM predictions at the catchment scale is impossible (Wilby *et al.*, 2004). However, as a method of bridging the coarse-resolution GCM outputs with catchment-scale hydroclimatic variables at finer resolutions, downscaling techniques have been developed (Chen *et al.*, 2010).

Downscaling techniques are broadly classified into the two categories of dynamic downscaling and statistical downscaling (Chu *et al.*, 2010). Dynamic downscaling involves nesting a finer resolution regional climatic model (RCM) in a coarse-resolution GCM (Murphy, 1998). The boundary conditions needed for the RCM to downscale the large-scale atmospheric conditions to catchment scale, are provided by the GCM. According to

Anandhi *et al.* (2008), dynamic downscaling suffers the drawbacks of high complexity and intense computational costs. The propagation of systematic bias from GCM to RCM is identified as another problem, associated with dynamic downscaling (Giorgi *et al.*, 2001). Unlike statistical downscaling, dynamic downscaling yields spatially distributed fields of climatic variables and it preserves certain spatial correlations and maintains physically realistic relationships between climatic variables (Maurer and Hidalgo, 2008). In statistical downscaling, statistical relationships are constructed between the coarse-resolution GCM outputs (predictors of downscaling models) and the catchment-scale hydroclimatic variables (predictands of downscaling models) (Chen *et al.*, 2010). Statistical downscaling involves low computational costs and can be implemented without detailed knowledge of the physical processes of the hydrologic cycle. In the process of statistical downscaling, the details of the geography of the study area are not needed, but in dynamic downscaling, a detailed knowledge of the geography is necessary. Although statistical downscaling possesses the above-mentioned advantages, a long time series of reliable observations is needed for model calibration and validation (Heyen *et al.*, 1996). A further consideration is that although statistical downscaling methods are much simpler than the dynamic downscaling methods, they could underestimate the variance and fail to reproduce the extreme events of hydroclimatic variables (Fowler *et al.*, 2007).

The major assumption in statistical downscaling is that the predictor–predictand relationships derived during the model development stage are valid for the future climatic conditions (Wilby and Wigly, 2000). Benestad *et al.* (2007) highlighted that, there exists a risk that a statistical downscaling method that performs well under present climate could fail under changing climate in future, simply due to the invalidity of the above-mentioned assumption. Statistical downscaling techniques are classified under three main categories of weather classification, regression models and weather generators (Wilby *et al.*, 2004). These three groups of methods are based on the concept that the local climate is mainly a function of the large-scale atmospheric conditions (Fowler *et al.*, 2007). In weather classification, predictor variables of GCMs are grouped into a number of states and the predictands are related to these states. Regression-based downscaling methods construct linear or nonlinear mathematical relationships between predictors and predictands (Chen *et al.*, 2010). Weather generators derive a synthetic series of climate data, preserving statistics of the corresponding observations (Wilks and Wilby, 1999).

Statistical downscaling of GCM predictors to catchment-scale hydroclimatic variables has gained wide application in the recent past. There are many examples in the literature of the use of statistical downscaling in climate prediction studies. Support vector machine (SVM) and artificial neural networks (ANNs) were used by Tripathi *et al.* (2006) for forecasting monthly precipitation. To predict daily precipitation, Chen *et al.* (2010) used

SVM and multi-linear regression (MLR). Anandhi *et al.* (2008, 2009) downscaled monthly precipitation and maximum/minimum temperatures with SVM. For downscaling daily mean temperature, Huth (2002) utilized MLR. Chu *et al.* (2010) downscaled daily mean temperature, pan evaporation and precipitation with linear regression. Salameh *et al.* (2009) applied generalized additive models (GAMs) to predict 6-h mean wind speeds. Timbal *et al.* (2009) used method of analogues to predict daily rainfall, minimum/maximum temperatures, pan evaporation and dew point temperature. Relative humidity, water vapour pressure, dew point temperatures and dew point deficits were downscaled using MLR by Huth (2005). Mean cloud cover, sunshine duration, relative humidity and minimum/maximum/mean temperatures were downscaled at the daily timescale by Enke and Spegat (1997) with the MLR technique. Cheng *et al.* (2008) applied MLR to downscale daily mean surface wind speed, mean sea-level pressure and minimum/maximum/mean temperatures. GAMs, generalized linear models, aggregated boosted trees and ANN were used for predicting daily streamflows by Tisseuil *et al.* (2010). Ghosh and Mujumdar (2008) implemented SVM and relevance vector machine to predict monthly streamflows. The ANN technique was utilized by Cannon and Whitfield (2002) for downscaling GCM outputs to 5-day mean streamflows. Seasonal streamflows were predicted by Landman *et al.* (2001) using canonical correlation analysis and perfect prognosis method.

A limited number of past investigations have been performed to directly downscale GCM predictors to streamflows. Direct downscaling of GCM predictors to streamflows using statistical downscaling methods allows for the forecasting of flows over larger regions under changing climate (Tisseuil *et al.*, 2010). In direct downscaling of GCM predictors to streamflows, influences of land use, soil cover and groundwater storage on streamflow are not considered (Xu, 1999), and it permits to make a quick estimate of streamflow. Furthermore, it skips the complicated hydroclimatic processes associated with streamflow generation in the natural hydrologic cycle, which ultimately leads to some errors. The direct downscaling method is only applicable to an unregulated streamflow site in a catchment, since the statistical functions derived between GCM outputs and streamflows are independent of any flow regulations imposed by humans.

The aim of the current study was to calibrate and validate least square SVM regression (LS-SVM-R) and MLR-based statistical downscaling models to downscale monthly GCM outputs directly to monthly streamflows. The two downscaling techniques were applied to a streamflow station of the Grampians water supply system in northwestern Victoria (Australia) as a case study. This article discusses the calibration and validation of the LS-SVM-R- and MLR-based streamflow prediction models and provides a comparison of the two techniques. The remainder of this article is organized as follows. The study area and data are described first, followed by the generic methodology. The application is then explained

leading to a discussion. Finally, the conclusions drawn from the study are presented.

2. Study area and data

The Grampians water supply system located in northwestern Victoria in Australia was selected as the study area for the current investigation. The Grampians system, owned and operated by Grampians Wimmera Mallee Water Corporation (GWMWater), is a large-scale multi-reservoir water supply system that supplies water for domestic, industrial, irrigation and environmental purposes. The prediction of streamflows in the Grampians system is a crucial task, since the system was severely battered by the recent Victorian drought during the period 1997–2008, which decreased inflows to the reservoirs of the system by about 75% from the long-term average. The prediction of future streamflow will allow the assessment of availability of water resources in the system and enhance the management of water within the system. Figure 1 depicts the location of the GWMWater operational area. The Grampians reservoir system is located in the south of the GWMWater operational area.

The present downscaling study was limited to a single streamflow site in the study region. The streamflow site is located on Fyans Creek at Lake Bellfield. The catchment area for this site is about 96 km² and situated wholly within a national park (GWMWater, 2011). Because of this location, land use has remained constant since European settlement in the 1800s. Geology of the catchment is predominantly sandstone with some deposits of mudstone (Cayley and Taylor, 1997). The quality of runoff is typically very good with low salinity, turbidity and moderate colour. The slope of the catchment is reasonably steep. Fyans Creek streamflows at Lake Bellfield are affected by diversions into, and out of, the catchment.

Monthly reanalysis data of National Center for Environmental Prediction/National Center for Atmospheric Research (NCEP/NCAR) and unregulated streamflow data at the site from 1950 to 2010 were used in the calibration and validation process of the downscaling models. These NCEP/NCAR reanalysis data (available from 1948 till today) are outputs of a GCM, corrected and quality controlled at several stages (Kalnay *et al.*, 1996). Many authors have used the NCEP/NCAR reanalysis data set for the calibration and validation of their downscaling models in the past (Tripathi *et al.*, 2006; Anandhi *et al.*, 2008, 2009; Ghosh and Mujumdar, 2008; Tisseuil *et al.*, 2010). The NCEP/NCAR reanalysis data are treated as an output of an ideal GCM (Cannon and Whitfield, 2002). The NCEP/NCAR reanalysis data were retrieved from the website (<http://www.esrl.noaa.gov/psd/>) of National Oceanic and Atmospheric Administration/Earth System Research Laboratory Physical Sciences Division. The quality-controlled unregulated monthly streamflow record at the site considered (inflow to Lake Bellfield in the Grampians system) in the present investigation was obtained from GWMWater. The unregulated inflow data

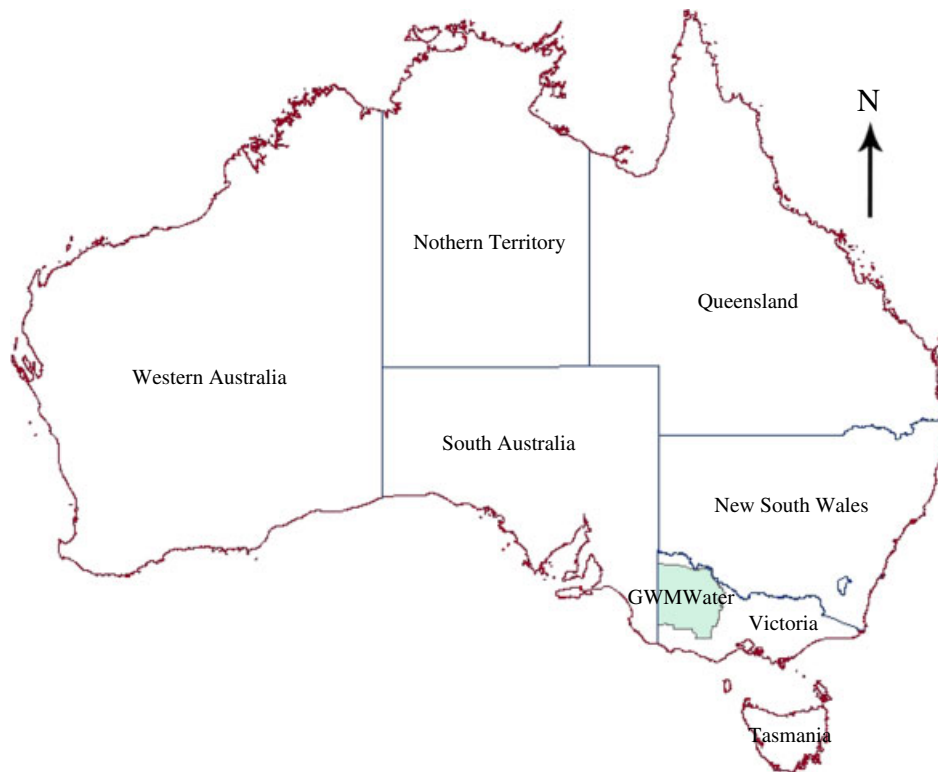


Figure 1. GWMWater operational area in northwestern Victoria, Australia.

to Lake Bellfield have been calculated using the water balance technique considering the upstream diversions (Sinclair, 2004).

3. Generic methodology

In statistical downscaling of GCM outputs to catchment-scale hydroclimatic variables, mathematical relationships are derived between the predictors and the predictand concerned, assuming the validity of these relationships under changing climate in future. In this study, predictor variables were extracted from the NCEP/NCAR reanalysis data archive, for downscaling them to monthly streamflows at the monitoring station. The downscaling models in this study were developed employing the LS-SVM-R and MLR techniques for each calendar month separately.

Initially, a substantially large atmospheric domain above and around the streamflow site was defined, as the climate and the hydrology at the site are influenced largely by this atmospheric domain. A pool of probable predictors was identified based on the past literature on statistical downscaling of GCM outputs to catchment streamflows and fundamentals of hydrology. The probable predictor pool consists of the GCM outputs, which have a high likelihood of influencing a certain predictand. These probable predictors are essentially a subset of all the predictors produced by a GCM (Anandhi *et al.*, 2008).

Potential predictors are a subset of probable predictors that vary for each season and for each streamflow

station. This is because the predictor–predictand relationships vary seasonally due to seasonal changes in atmospheric circulations (Karl *et al.*, 1990) and also with the geography. These potential predictors were the most influential variables on streamflow generation during a certain season or a calendar month. In the past downscaling studies, models based on, the calendar months (Najafi *et al.*, 2011), the wet and dry seasons (Chen *et al.*, 2010) and the four traditional seasons summer, autumn, winter and spring (Timbal *et al.*, 2009) have been employed. In the present statistical downscaling exercise, models were developed for each calendar month to capture the seasonal variability of the streamflow with a higher degree of accuracy. Therefore, each calendar month had its own pool of potential variables. To obtain the potential variables for each calendar month from the pool of probable variables, the Pearson correlation coefficient (Pearson, 1895) was used. For identifying potential variables from the probable variable pool, Tripathi *et al.* (2006) and Anandhi *et al.* (2008) used correlation coefficient analysis successfully. The record of monthly streamflow data and the probable predictors were split, chronologically into 20-year time slices. For each 20-year time slice, the Pearson correlation coefficients between each predictor at each grid point of the atmospheric domain and the streamflow were calculated, for each calendar month. Similarly, the Pearson correlation coefficients, between each predictor at each grid point of the atmospheric domain and the streamflow for the entire period covering all the 20-year time slices were calculated. After this process, the probable predictors that displayed the best

Pearson correlation coefficients over the entire period of data, while exhibiting good correlation coefficients consistently over all 20-year time slices, were selected as the potential predictors for each month. The consistency of the correlation between a predictor and streamflow was important since a good predictor of a predictand should show a consistent relationship over time. By splitting the data into 20-year time slices, any predictor that exhibited inconsistencies in correlations with streamflows over time could be identified, and subsequently eliminated.

The first two thirds of the predictor and streamflow data time series were allocated for the model calibration, and the remaining one third of the data was allocated for the model validation. The above-selected potential predictors for the model calibration period were standardized for each calendar month by subtracting the means and dividing by the standard deviations corresponding to the same period. The standardization of the potential predictors in the validation phase was performed with the means and standard deviations corresponding to the calibration period of the data set. The standardization of NCEP/NCAR predictors scaled down the predictor data to a single uniform scale and removed the units of the variables. This process was widely practised in many of the downscaling studies in the past (Tripathi *et al.*, 2006; Anandhi *et al.*, 2008, 2009; Ghosh and Mujumdar, 2008; Chen *et al.*, 2010).

The LS-SVM-R- and MLR-based model calibration and validation were conducted for each calendar month by introducing the standardized potential predictors to the models. The introduction of the standardized potential predictors to these models was done by initially ingesting the first three best correlated predictors and then the next best correlated predictors one by one, until the model performance was maximized for validation. The model parameters were obtained by comparing the model predictions with observations. The LS-SVM-R-based models were calibrated with the leave-one-out cross-validation and the model parameter optimization was performed using the simplex algorithm proposed by Nelder and Mead (1965). The MLR-based downscaling model parameter optimization was achieved by minimizing the sum of the squares of the errors. The stepwise development of the downscaling models enabled the selection of the optimum number of potential variables for each calendar month. These optimum potential predictors were a small subset of potential variables, which maximized the model performance in the validation phase, for the calendar month. The model validation was conducted as a simulation independent of calibration by fixing the optimum model parameters obtained in the calibration. The model performances in calibration and validation during each calendar month and four seasons were measured using the original Nash–Sutcliffe (N-S) efficiency formula defined by Nash and Sutcliffe (1970). Both original N-S efficiency and seasonally adjusted Nash–Sutcliffe (SANS) efficiency proposed by Wang (2006) were computed for the estimation of the model performance over the entire calibration and validation

period, covering all four seasons and years. In the calculation of N-S efficiency, the original N-S formula uses the overall average of the streamflows irrespective of seasons or months considered, whereas the SANS efficiency formula uses the individual seasonal averages of streamflows in the same N-S formula. When there is a considerable difference between the overall average of the streamflow and the individual seasonal averages of the streamflows, the original N-S formula tends to produce overall model performance values higher than those of four seasons (Wang, 2006). However, due to the inclusion of seasonal averages of streamflows, SANS efficiency formula produces overall model performances, which are comparable with those of seasons.

In general, predictor variables are highly correlated over the spatial domain from which they are obtained (Ghosh and Mujumdar, 2008). This could introduce redundant information into the statistical downscaling model, making it unstable and unnecessarily complicated. Principal component (PC) analysis has been used in the past downscaling studies to extract the variance present in a large standardized predictor variable set to a limited number of PCs (Tripathi *et al.*, 2006; Anandhi *et al.*, 2008, 2009; Ghosh and Mujumdar, 2008). To determine how effective the use of PCs, in comparison with the raw standardized predictor data, as the inputs to a statistical downscaling model, an additional investigation was performed. In this investigation, PCs were extracted only for two calendar months from the standardized optimum potential predictors. The first few PCs that explained about 98% of the variance in the original optimum potential predictors were introduced to the LS-SVM-R model. The PC-based LS-SVM-R models were calibrated and validated, and their performances were compared with those of the aforementioned corresponding non-PC models. It was assumed that PC-based models developed with the LS-SVM-R technique will perform similar to those with MLR. Owing to this, PC-based models were not developed with the MLR technique in this study.

3.1. Overview of LS-SVM-R

The SVM is a machine learning algorithm with potential for classification and function approximation using regression (Basak *et al.*, 2007). SVM was initially developed for classification, but the theory was extended for function estimation in 1996 (Drucker *et al.*, 1996). Vapnik (2000) provides a detailed description on the SVM theory, accounting for both classification and regression. LS-SVM is a simplified version of the original SVM algorithm for classification and function estimation, which maintains the advantages and the attributes of the original SVM theory (Suykens *et al.*, 2002). According to Suykens and Vandewalle (1999), LS-SVM possesses excellent generalization performances and is associated with low computational costs. LS-SVM requires less effort in model training in comparison to the original SVM, owing to its simplified algorithm (Zhou *et al.*, 2011). Due to these advantages, LS-SVM-R was

employed in this study. Tripathi *et al.* (2006), Anandhi *et al.* (2009) and Zhou *et al.* (2011) applied LS-SVM-R successfully for downscaling GCM outputs to catchment-scale climatic variables.

The theory of LS-SVM is discussed in detail by Suykens *et al.* (2002). The following is a brief account on the theory of LS-SVM-R. Consider the sample (X, Y) , where X is the independent variable, $X_i \in \mathcal{R}^n$ and $X = [X_1, X_2, X_3 \dots X_i \dots X_n]$. Y is the dependent variable where $Y_i \in \mathcal{R}$.

Consider a model of the following form in Equation (1), where w are the model coefficients and $\varphi(\cdot)$ is the function used for mapping the data of X into a high-dimensional feature space:

$$Y(X) = w^T \varphi(X) + b \tag{1}$$

The LS-SVM-R optimization problem could be written as follows:

$$\min \Psi(w, e) = \frac{1}{2} w^T w + \frac{1}{2} \gamma \sum_{i=1}^n e_i^2 \tag{2}$$

where Ψ is the cost function to be minimized.

$$\text{subject to the constraint } Y_i = w^T \varphi(X_i) + b + e_i \tag{3}$$

where e is the error and γ the regularization parameter.

The Lagrangian solution to the above-mentioned optimization is given by the following equation:

$$L(w, e, b, \alpha) = \frac{1}{2} w^T w + \frac{1}{2} \gamma \sum_{i=1}^n e_i^2 - \sum_{i=1}^n \alpha_i \{w^T \varphi(X_i) + b + e_i - Y_i\} \tag{4}$$

L is the Lagrangian function in which α_i are the Lagrangian multipliers. Conditions for the optimality of Equation (4) are given by the following equations:

$$\frac{\partial L}{\partial w} = 0, \rightarrow w = \sum_{i=1}^n \alpha_i \varphi(X_i) \tag{5}$$

$$\frac{\partial L}{\partial b} = 0, \rightarrow \sum_{i=1}^n \alpha_i = 0 \tag{6}$$

$$\frac{\partial L}{\partial e_i} = 0, \rightarrow \alpha_i = \gamma e_i \text{ For all } i \tag{7}$$

$$\frac{\partial L}{\partial \alpha_i} = 0, \rightarrow w^T \varphi(X_i) + b + e_i - Y_i = 0 \text{ For all } i \tag{8}$$

After eliminating w and e from the above conditions (from Equations (5), (6), (7), and (8)), the following equation is obtained:

$$\begin{bmatrix} 0 & 1_v^T \\ 1_v & \Omega + I\gamma^{-1} \end{bmatrix} \begin{bmatrix} b \\ \alpha \end{bmatrix} = \begin{bmatrix} 0 \\ Y \end{bmatrix} \tag{9}$$

where

$$Y = \begin{bmatrix} Y_1 \\ Y_2 \\ \vdots \\ Y_n \end{bmatrix}, \quad 1_v = \begin{bmatrix} 1 \\ 1 \\ \vdots \\ 1 \end{bmatrix}, \quad \alpha = \begin{bmatrix} \alpha_1 \\ \alpha_2 \\ \vdots \\ \alpha_n \end{bmatrix},$$

$$I = \begin{bmatrix} 1 & 0 & \dots & 0 \\ 0 & 1 & \dots & 0 \\ \vdots & \vdots & \dots & \vdots \\ 0 & 0 & \dots & 1 \end{bmatrix}, \quad \Omega_{ij} = \varphi(X_i)^T \varphi(X_j)$$

and $\Omega_{ij} = K(X_i, X_j)$ is the kernel function (10)

The LS-SVM-R model becomes $Y(X) = \sum_{i=1}^n \alpha_i K(X_i, X_j) + b$ in which α and b can be found by solving Equation (9).

When the radial basis function (RBF) is used as the kernel, where $K(X_i, X_j) = \exp(-\|X_i - X_j\|^2 / 2\sigma^2)$, the LS-SVM-R tuning parameters become γ and σ (width of the RBF kernel). In this study, the above-described LS-SVM-R technique was used for downscaling NCEP/NCAR predictors to streamflows. For LS-SVM regression, LS-SVMlab 1.7 toolbox (De Brabanter *et al.*, 2010) was downloaded free from <http://www.esat.kuleuven.be/sista/lssvmlab/> and implemented in MATLAB (R2008b) environment.

3.2. Overview of MLR

MLR is an extension of simple linear regression, where multiple independent variables are used in explaining the behaviour of the dependent variable. MLR is used to build mathematical functions between two or more independent variables and a dependent variable, by fitting linear equations to a set of observed data. The best fit line is determined by minimizing the sum of the squares of the vertical deviations (residuals) between the line and the observed data. A good MLR model should be able to explain most of the variance of the dependent variable with the minimum number of independent variables (Helsel and Hirsch, 2002). The MLR technique is given by the following equation:

$$Y = \beta_0 + \beta_1 X_1 + \beta_2 X_2 + \beta_3 X_3 + \dots + \beta_i X_i + \dots + \beta_n X_n + \varepsilon \tag{11}$$

where Y is the dependent variable (predictand in a downscaling exercise), β_0 the intercept, β_i the coefficient of the i th independent variable X_i (i th predictor in a downscaling exercise) and ε the noise in data. A detailed description on the theory of MLR is provided by Helsel and Hirsch (2002). This study employed the MLR technique for downscaling NCEP/NCAR predictors to streamflows, in parallel with LS-SVM-R. The MLR option in the statistics toolbox in MATLAB (R2008b) was used to build the MLR-based downscaling models.

4. Application

The generic methodology described in Section 3 was applied to the streamflow site in the Grampians water supply system as a demonstration.

4.1. Atmospheric domain for downscaling

In the past, many authors in their downscaling studies defined large atmospheric domains over and around the points concerned on the ground. An atmospheric domain of 5×5 grid points was defined by Ghosh and Mujumdar (2008) in downscaling GCM outputs to streamflows, while Tripathi *et al.* (2006) and Anandhi *et al.* (2008) used 6×6 and 3×3 grid arrangements, respectively, for downscaling GCM predictors to precipitation. Although there is no guideline on the selection of the optimum atmospheric domain size, a substantially larger domain will enable to determine greater number of better correlations between the predictors and the predictand. The main drawback of a large atmospheric domain is the increased computational cost. This study employed a large atmospheric domain of 7×6 grid points, each 2.5° apart, over the streamflow station as shown in Figure 2. The grid points were maintained 2.5° apart to make this grid compliant with the resolution of the NCEP/NCAR reanalysis data.

4.2. Probable and potential predictors for downscaling

The performances of a statistical downscaling model are dependent on the choice of predictors and the selection of

the atmospheric domain (Wilby and Wigly, 1997). In any downscaling study, the selection of predictors should be given high priority (Fowler *et al.*, 2007). A clear understanding of the physics of predictors and their connections to the predictand aids the proper selection of a predictor variable set, relevant to a certain downscaling exercise. For the present downscaling exercise, 23 probable predictors were selected from the NCEP/NCAR reanalysis data set based on the literature on similar studies and hydrology. These probable predictors were common for all calendar months. Each of these predictors had a spatial dimension of 7×6 over the atmospheric domain, as shown in Figure 2. The 23 probable predictors and the basis of their selection are given in Table I.

The next step was to extract potential predictors from the probable predictor pool for each calendar month. The record of streamflows and NCEP/NCAR probable predictors from 1950 to 2010 were separated into three 20-year time slices 1950–1969, 1970–1989 and 1990–2010. It is noteworthy to mention that the last time slice spanning 1990–2010 was 21 years in length. For each of these time slices and for the entire study period (1950–2010), the Pearson correlation coefficients between each probable predictor at each grid point in the atmospheric domain and streamflow were calculated. The probable variables that showed the best, statistically significant (95 % confidence level, $p = 0.05$) correlations with the streamflow, consistently over the above-mentioned three 20-year time

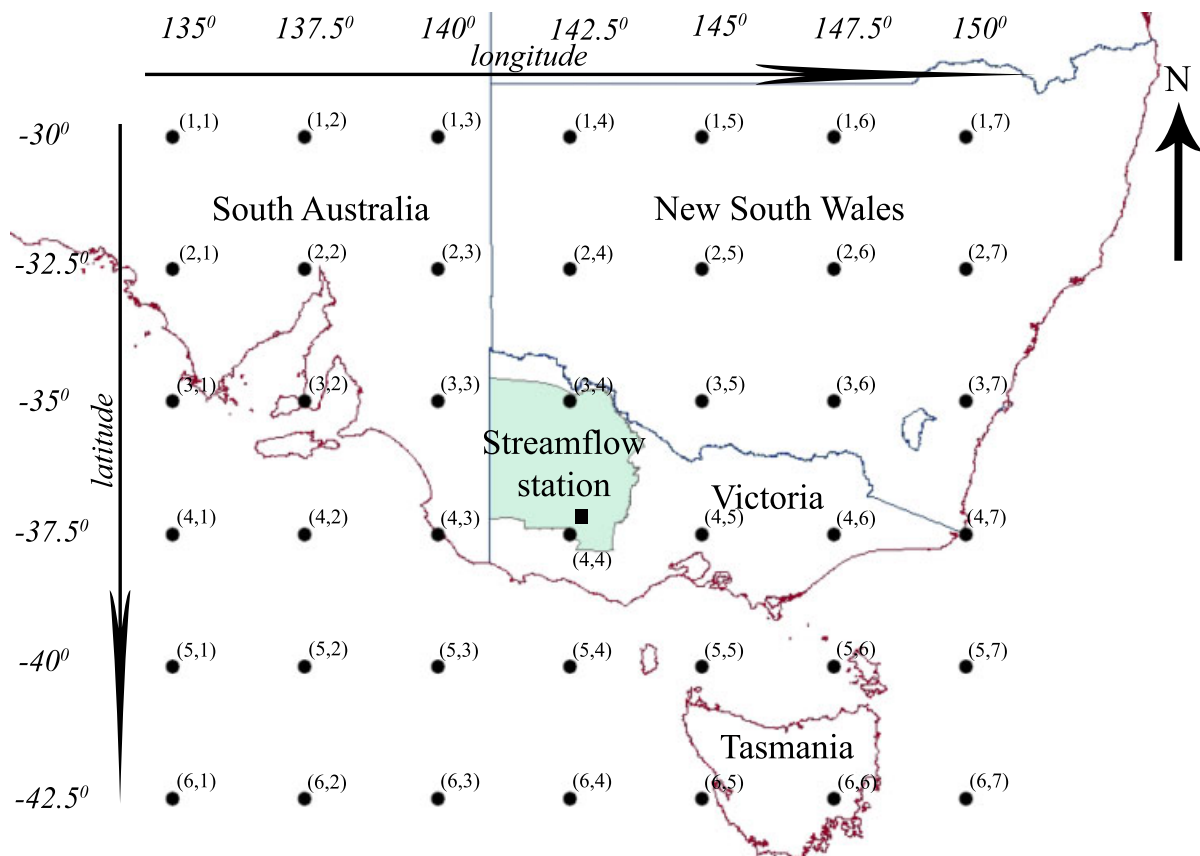


Figure 2. Atmospheric domain defined over the streamflow station.

Table I. Probable predictors used in the study.

Name of predictor	Basis of selection
200 hPa geopotential height	Landman <i>et al.</i> (2001)
500 hPa geopotential height	Landman <i>et al.</i> (2001), Cannon and Whitfield (2002), Ghosh and Mujumdar (2008), Tisseuil <i>et al.</i> (2010)
700 hPa geopotential height	Landman <i>et al.</i> (2001)
850 hPa geopotential height	Landman <i>et al.</i> (2001), Tisseuil <i>et al.</i> (2010)
1000 hPa geopotential height	Tisseuil <i>et al.</i> (2010)
500 hPa relative humidity	Tisseuil <i>et al.</i> (2010)
700 hPa relative humidity	Landman <i>et al.</i> (2001)
850 hPa relative humidity	Tisseuil <i>et al.</i> (2010)
1000 hPa relative humidity	Tisseuil <i>et al.</i> (2010)
2 m specific humidity	Ghosh and Mujumdar (2008)
500 hPa specific humidity	Tisseuil <i>et al.</i> (2010)
850 hPa specific humidity	Cannon and Whitfield (2002), Tisseuil <i>et al.</i> (2010)
1000 hPa specific humidity	Tisseuil <i>et al.</i> (2010)
2 m air temperature	Ghosh and Mujumdar (2008)
Surface air temperature	Ghosh and Mujumdar (2008)
Surface skin temperature	Tisseuil <i>et al.</i> (2010)
500 hPa air temperature	Tisseuil <i>et al.</i> (2010)
850 hPa air temperature	Tisseuil <i>et al.</i> (2010)
1000 hPa air temperature	Tisseuil <i>et al.</i> (2010)
Surface pressure	Tisseuil <i>et al.</i> (2010)
Mean sea-level pressure	Cannon and Whitfield (2002), Ghosh and Mujumdar (2008), Tisseuil <i>et al.</i> (2010)
Volumetric soil moisture content 0–10 cm	Hydrology
Volumetric soil moisture content 10–200 cm	Hydrology

hPa = atmospheric pressure in hectopascal.

slices and the whole period, were selected as potential variables, for each calendar month.

As an example of selecting the final set of potential predictors for a calendar month from the pool of probable variables, Table II shows the potential predictors with their grid locations (according to Figure 2) used as the final inputs to the LS-SVM-based downscaling model in January.

The predictors that displayed correlations (with streamflow), either consistently positive or negative and having reasonably similar magnitudes, over the three time slices and the whole study period were ranked in the descending order, according to the magnitude of the correlation corresponding to the whole study period. In other words, the predictors that displayed correlations with fluctuating signs (positive to negative or vice versa) and largely varying magnitudes over time were excluded from the potential variable set of a certain calendar month. These predictors were introduced to the downscaling model, initially, the first three predictors with the best correlations and the next best predictors one at a time, to the previous set of potential predictors. In January, the best three potential variables, the 1000 hPa relative humidity at 1,2; 2,2 and 2,3 grid locations with correlation coefficients of 0.61, 0.57 and 0.54, respectively, were initially input to the downscaling model. Thereafter the potential variables with rank 4, 5, 6 etc. were introduced to the model one at a time. This stepwise introduction of predictors was performed until the model performances in the validation

were maximized. With the addition of the eighth variable (volumetric soil moisture content 10–200 cm at 4,4), the January LS-SVM model displayed the best performance in validation in terms of the N-S efficiency. The addition of the ninth and other ranked variables (these variables have not been shown in Table II) did not improve the model performances in validation. Therefore, the final set of potential variables for the January LS-SVM model was limited to eight variables. This procedure was practised for all calendar months, with both LS-SVM and MLR models, in extracting the potential variables. Table III shows the potential variables used for the LS-SVM and MLR models for each calendar month.

The final sets of potential predictors shown in Table III for each calendar month, used in LS-SVM and MLR models, consisted of 850 hPa air temperature, 850 hPa specific humidity, volumetric soil moisture contents in 0 to 10 cm and 10 to 200 cm soil layers; 700 hPa, 850 hPa and 1000 hPa relative humidities and 500 hPa, 700 hPa and 850 hPa geopotential heights. Streamflow generation is a result of a series of complex hydroclimatic processes such as precipitation, evaporation and infiltration. However, precipitation is regarded as the most prominent force of generation of streamflows. In a statistical downscaling study performed by Timbal *et al.* (2009), it has been found that 850 hPa air temperature and 850 hPa specific humidity are potential predictors of precipitation over southwest of eastern Australia, which covers the current study area. Hence, it was understood that 850 hPa

Table II. Potential predictors used for the January LS-SVM model and their correlations with streamflows in each time slice and whole period.

Rank of the variable	Potential variables for January	Grid location	Time slice	Correlation with streamflow
1	1000 hPa relative humidity	2,3	1950–1969	0.45
			1970–1989	0.68
			1990–2010	0.56
			1950–2010	0.61
2	1000 hPa relative humidity	2,2	1950–1969	0.23
			1970–1989	0.61
			1990–2010	0.56
			1950–2010	0.57
3	1000 hPa relative humidity	1,2	1950–1969	0.22
			1970–1989	0.66
			1990–2010	0.45
			1950–2010	0.54
4	1000 hPa relative humidity	4,3	1950–1969	0.41
			1970–1989	0.47
			1990–2010	0.59
			1950–2010	0.51
5	1000 hPa relative humidity	3,3	1950–1969	0.30
			1970–1989	0.45
			1990–2010	0.57
			1950–2010	0.50
6	Volumetric soil moisture content 10–200 cm	2,2	1950–1969	0.38
			1970–1989	0.47
			1990–2010	0.56
			1950–2010	0.47
7	Volumetric soil moisture content 0–10 cm	2,2	1950–1969	0.32
			1970–1989	0.49
			1990–2010	0.57
			1950–2010	0.43
8	Volumetric soil moisture content 10–200 cm	4,4	1950–1969	0.23
			1970–1989	0.51
			1990–2010	0.51
			1950–2010	0.42

air temperature and 850 hPa specific humidity are potential predictors of the streamflows, over this study area. The soil moisture content (in this study the moisture in the 0 to 10 cm and 10 to 200 cm soil layers) is a governing factor, which decides how much of the precipitation is converted to runoff. Therefore, the soil moisture content was treated as an important potential predictor of streamflow. Relative humidities at various pressure levels are indicators of the atmospheric water vapour content leading to the formation of clouds, which will finally contribute to precipitation. Therefore, the relative humidities at various pressure levels, which displayed good correlations with the streamflow were remained in the pools of potential predictors. Geopotential heights depict the heights of the pressure surfaces of equal pressure above the mean sea level. These geopotential heights are indicators of atmospheric troughs and ridges (Cosma *et al.*, 2002), which are related with relatively low and relatively high atmospheric pressure fields causing rainfall and relatively dry weather conditions, respectively. Therefore, various geopotential heights that showed a good relationship with streamflows were included in the sets of potential predictors.

4.3. Inputs for model calibration and validation

The inputs to the LS-SVM-R- and MLR-based models for the calibration and validation were the same, as these two modelling approaches were applied in parallel. The time series of streamflow and predictor data, which covered the 40-year period spanning 1950–1989, was selected for the model calibration. The rest of the 21-year long data record from 1990 to 2010 was used for the model validation. The potential predictors identified in Section 4.2 were used to generate inputs for the downscaling model. The potential predictors for the model calibration were standardized with the means and the standard deviations corresponding to period 1950–1989. The inputs for model validation were produced by standardizing the potential predictors from 1990 to 2010, with the means and the standard deviations pertaining to period 1950–1989. This procedure was practised in the standardization of predictors for the model validation, since the means and standard deviations of the predictors corresponding the calibration period are a stationary component of the statistical downscaling models, employed in this study. The same means and standard deviations will be used in the projection of future streamflows. The

Table III. Potential predictors used in the LS-SVM and MLR models for each calendar month.

Month	Potential variables used for LS-SVM model with grid locations	Potential variables used for MLR model with grid locations
January	1000 hPa relative humidity {(1,2),(2,2),(2,3),(3,3),(3,4)} Volumetric soil moisture content 0–10 cm {(2,2)} Volumetric soil moisture content 10–200 cm {(2,2),(4,4)}	1000 hPa relative humidity {(1,2),(2,2),(2,3),(3,4)}
February	Volumetric soil moisture content 0–10 cm {(4,3)} Volumetric soil moisture content 10–200 cm {(2,2),(3,1),(3,2)}	Volumetric soil moisture content 0–10 cm {(4,3)} Volumetric soil moisture content 10–200 cm {(2,2),(3,1),(3,2)}
March	1000 hPa relative humidity {(5,6),(5,7),(6,6),(6,7)}	1000 hPa relative humidity {(5,6),(6,6),(6,7)}
April	700 hPa relative humidity {(4,2),(4,3)} 850 hPa relative humidity {(4,2),(5,2)}	700 hPa relative humidity {(4,2),(4,3)} 850 hPa relative humidity {(4,2)}
May	Volumetric soil moisture content 0–10 cm {(4,2),(4,3),(4,4),(4,5),(5,3),(5,4),(5,5)} 850 hPa air temperature {(3,1)}	Volumetric soil moisture content 0–10 cm {(4,3),(4,4),(4,5)}
June	Volumetric soil moisture content 0–10 cm {(4,3),(4,4), (5,3),(5,4)} 500 hPa geopotential height {(4,2)}	Volumetric soil moisture content 0–10 cm {(4,3),(4,4),(5,2),(5,3),(5,4),(6,3)} 500 hPa geopotential height {(4,2)}
July	700 hPa geopotential height {(4,4)} 850 hPa geopotential height {(4,4),(4,5)}	700 hPa geopotential height {(4,4)} 850 hPa geopotential height {(4,3),(4,4),(4,5)}
August	700 hPa geopotential height {(5,3),(5,4),(5,5),(5,6)} 850 hPa geopotential height {(4,5),(5,4),(5,5),(5,6)}	700 hPa geopotential height {(5,4),(5,5)} 850 hPa geopotential height {(5,4),(5,5),(5,6)}
September	700 hPa geopotential height {(2,1),(2,2),(3,2),(3,3)}	700 hPa geopotential height {(2,1),(3,2),(3,3)}
October	Volumetric soil moisture content 0–10 cm {(4,2),(4,3),(4,4), (5,2),(5,3),(5,4),(6,3)}	Volumetric soil moisture content 0–10 cm {(4,3),(4,4),(5,3)}
November	700 hPa geopotential height {(2,2),(2,3),(2,4),(3,2),(3,3),(3,4)} 500 hPa geopotential height {(2,3)}	700 hPa geopotential height {(2,2),(2,3),(2,4),(3,2),(3,3),(3,4)}
December	700 hPa relative humidity {(4,3)} 850 hPa relative humidity {(3,1)} 1000 hPa relative humidity {(6,6)} 850 hPa specific humidity {(5,5)} Volumetric soil moisture content 0–10 cm {(4,4),(4,5),(5,4)} Volumetric soil moisture content 10–200 cm {(3,2),(4,3),(4,4)}	700 hPa relative humidity {(4,3)} 850 hPa relative humidity {(3,1)} 1000 hPa relative humidity {(6,6)} 850 hPa specific humidity {(5,5)} Volumetric soil moisture content 0–10 cm {(4,4),(4,5),(5,4)} Volumetric soil moisture content 10–200 cm {(3,2),(4,3),(4,4)}

observed streamflow data used in the model calibration and validation were not standardized as streamflow was the only predictand of the models.

4.4. LS-SVM-R downscaling model calibration and validation

The LS-SVM-R models employed in this downscaling study had two tuning parameters γ and σ , where γ is the regularization parameter and σ is the width of the RBF kernel. The kernel function in LS-SVM-R is utilized in mapping the nonlinear predictor–predictand relationship to a linear relationship in a higher dimensional space. In the past downscaling studies performed by Tripathi *et al.* (2006), Anandhi *et al.* (2008) and Ghosh and Mujumdar (2008), it was found that the RBF kernel

performs superior to the other kernels such as linear and polynomial, and therefore, this study employed the RBF kernel.

The standardized potential variables for each calendar month were introduced to the LS-SVM-R models, initially the three potential predictors that showed the best correlation coefficients and thereafter the next best predictors, one at a time. With each addition of a new predictor, the model performances in calibration and validation were monitored with the original N-S efficiency formula. The model that displayed the best N-S efficiency in validation was selected as the best model for the calendar month. The SANS efficiency was used to estimate the overall model performance during calibration and validation, along with the original N-S efficiency. All the

model performances were monitored using the raw values of observed and predicted streamflows. Scatter and time series plots were graphed to produce visual comparisons of model predicted streamflows with observed flow. The model validation was conducted as a simulation in which the optimum values of γ and σ yielded in the calibration remained fixed. The same process was followed for all calendar months.

January and December had eight and ten optimum number of potential predictors to LS-SVM-R models, respectively. The PC analysis was used to derive PCs related to these predictors of the two months. The first five and seven PCs that covered about 98% of the variance of the original potential variables, were introduced initially to the LS-SVM-R January and December downscaling models. Thereafter, the number of input PCs to the model was increased one at a time until all PCs were introduced. The coefficients of these PCs extracted for the model calibration were used in the generation of PCs for the validation phase, as these coefficients of PCs become a part of the model in future predictions. The same parameter optimization and calibration and validation procedures described above for non-PC LS-SVM-R models were applied to PC-based models.

4.5. MLR downscaling model calibration and validation

The same model calibration and validation procedure described under Section 4.4 was employed in the MLR-based model development. The MLR model optimization was performed by minimizing the sum of the squares of the errors, between the model predictions and observations. The optimum number of model inputs to the MLR downscaling models was different from that of LS-SVM-R models, for a calendar month. This was since, for the same calendar month, the two types of models needed different numbers of predictors (different predictor combinations) to exhibit the maximum performance in validation.

4.6. Results of LS-SVM-R-based downscaling model calibration and validation

Figure 3 displays the comparison of observed monthly flow and the monthly flow predicted by the LS-SVM-R

downscaling model for the calibration (1950–1989) and validation (1990–2010) periods.

To produce this plot of streamflow time series, the outputs of each individual calendar month-based model were combined sequentially from 1950 to 2010. During the calibration phase from 1950 to 1989, the LS-SVM-R downscaling model showed an N-S efficiency of 0.73, and in the validation phase from 1990 to 2010, an N-S efficiency of 0.47 was observed. The overall SANS efficiencies for the calibration and validation of the LS-SVM-R model were 0.59 and 0.27, respectively. In the model calibration, the observed average streamflow of 2129.3 ML month⁻¹ was well reproduced by the model as 2130 ML month⁻¹, but during the validation, the observed average streamflow of 1318.5 ML month⁻¹ was over-estimated by the model as 1910 ML month⁻¹. The year 1997 was the start of a long drought in Victoria, which lasted until mid-2010. In the time series plot in Figure 3, a distinct over-prediction of high streamflows by the LS-SVM-R model was observed after 1997, where a drop in the average of the observed streamflow was evident. The observed average of the streamflows at the monitoring site showed a 56% reduction in the post-1997 era with respect to the flow average for the period 1950–1996.

The scatter plots corresponding to the calibration and validation phases of the LS-SVM-R-based downscaling models are shown in Figure 4. According to the scatter plots, during calibration, the LS-SVM-R model under-predicted the majority of high flows, meanwhile in validation, it tended to over-predict most of the streamflows. In both calibration and validation, the LS-SVM-R model failed to predict most of the zero and low flows correctly, and in certain instances, it heavily over-predicted the zero flows, mainly during the validation period. In the observed flow record, 1.5% of the streamflow data were zero flows during the calibration period, and the zero flow percentage was about 7.3% in the validation period.

Figure 5 depicts the scatter plots for each season under the calibration and validation phases of the LS-SVM-R-based models. The summer, autumn, winter and spring were defined as periods December–February,

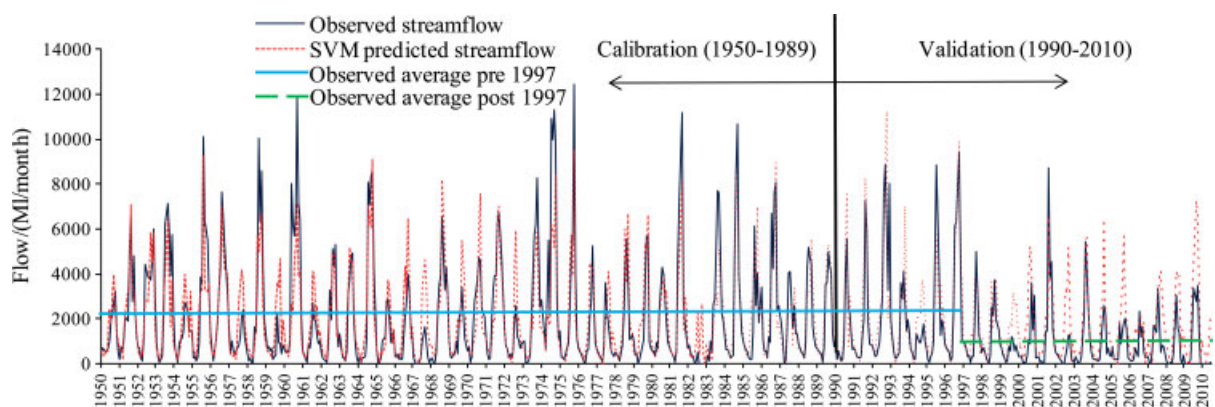


Figure 3. Observed streamflow and SVM-predicted streamflow.

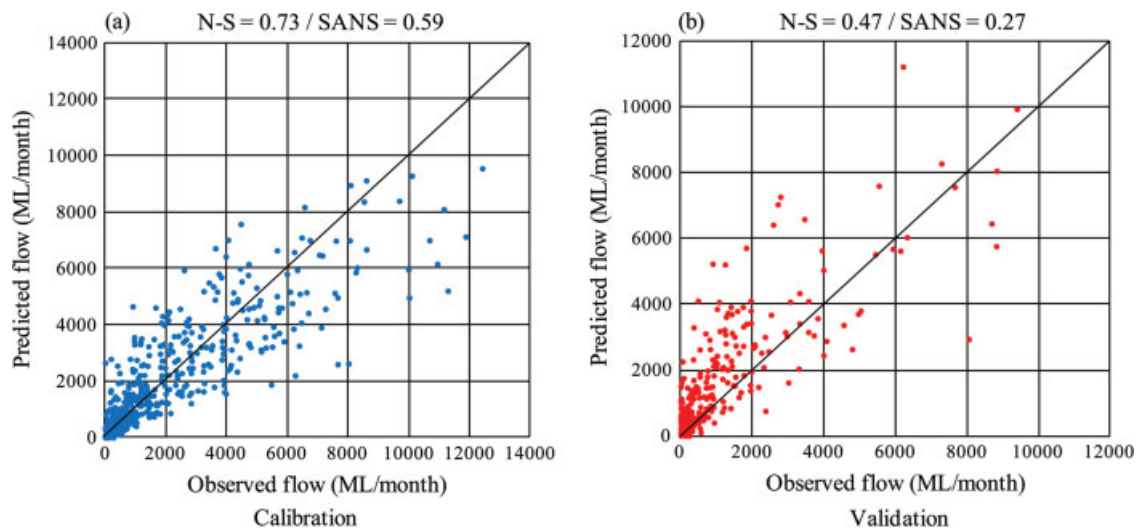


Figure 4. Scatter plots for calibration and validation phases of SVM-based model.

March–May, June–August and September–November, respectively. Good calibration results were observed in winter and summer with N-S efficiencies of 0.56 and 0.55, and the same two seasons exhibited the best N-S efficiencies of 0.38 and 0.39, respectively, of all seasons in LS-SVM-R model validation. In autumn, the model validation failed drastically with a poor N-S efficiency of -2.45 , though the autumn calibration was performed with a reasonably good N-S efficiency of 0.45. Extremely high over-estimation of zero and low flows was observed in the autumn validation. The spring calibration yielded the best N-S efficiency of all the four seasons of 0.62, but in validation, the model accuracy slumped to an N-S efficiency of 0.16. For all the four seasons, the LS-SVM-R model had a trend of under-predicting higher streamflows during the calibration phase, and in validation, the trend was more an over-predicting one for the majority of streamflows.

4.7. Results of MLR-based downscaling model calibration and validation

Figure 6 shows the comparison of observed and MLR downscaling model predicted monthly streamflows for the calibration (1950–1989) and validation (1990–2010) periods.

The MLR-based downscaling strategy displayed a trend of largely over-predicting the high streamflows particularly after 1997 of the validation phase. The results of the MLR model showed an N-S efficiency of 0.69 during the calibration period and 0.33 in the validation period. The corresponding SANS efficiencies for the MLR model calibration and validation were 0.54 and 0.08, respectively. In calibration, MLR-based downscaling models tended to under-predict most of the high flows, and in validation, the majority of streamflows were over-estimated. The observed mean streamflow of $2129.3 \text{ ML month}^{-1}$ during the calibration was correctly reproduced by the MLR-based model as $2132 \text{ ML month}^{-1}$, while the observed mean streamflow of $1318.5 \text{ ML month}^{-1}$ in

the validation was over-estimated as $2018 \text{ ML month}^{-1}$. Figure 7 is a scatter plot representation of the streamflows generated by the MLR model, which provides pictorial evidence on under-prediction and over-prediction of streamflows in calibration and validation, respectively.

Figure 8 illustrates the seasonal scatter plots of the MLR-based downscaling models, for the calibration and validation phases. During summer calibration and validation, the MLR-based models displayed the best N-S efficiencies of 0.60 and 0.50, respectively, for all the four seasons. The MLR model showed an N-S efficiency of 0.38 in autumn calibration, but failed largely in predicting the autumn streamflows in the validation phase producing an N-S efficiency of -3.70 . In autumn validation, the MLR model clearly over-estimated the majority of the streamflows. In winter, the MLR model attained N-S efficiencies of 0.59 and 0.19 in calibration and validation, respectively. During spring, the MLR model was calibrated with an N-S efficiency of 0.51, but a poor N-S efficiency of -0.09 was observed in model validation. For all the four seasons, during calibration, the MLR-based model had a tendency of under-predicting most of the high flows. In validation, the majority of flows were over-predicted by MLR for all the four seasons.

4.8. Comparison of LS-SVM-R and MLR downscaling approaches

The results of this study provided a platform for a comparison of the potential of LS-SVM-R (which is a complex nonlinear downscaling technique) and MLR (which is a less complicated linear downscaling technique) for the prediction of monthly streamflows. The streamflow data used in the calibration period from 1950 to 1989 referred to a relatively wetter climatic regime, while the flow data used for the model validation was under a relatively dryer climatic regime, especially after 1997, when the recent drought in Victoria commenced. Furthermore, the observed streamflow data had a larger scatter in the

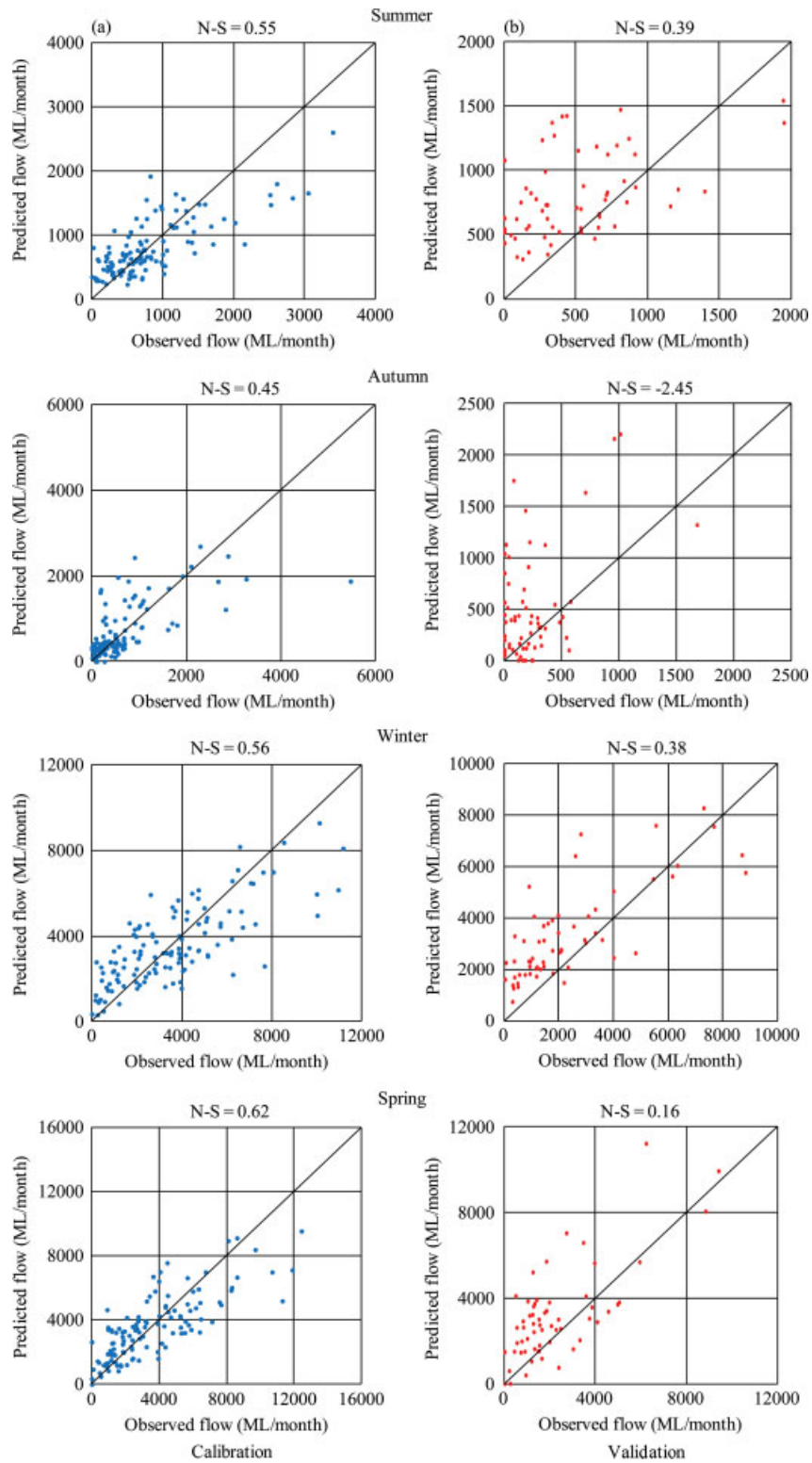


Figure 5. Seasonal scatter plots for calibration (left) and validation (right) of SVM-based model.

validation with a coefficient of variation of 1.36, than in the calibration, in which the coefficient of variation was 1.12. Table IV shows the statistical comparison of the performances of the two modelling approaches in the calibration and validation phases, together with the attributes of the observed streamflows.

During the calibration phase (1950–1989) of the models, both LS-SVM-R and MLR techniques produced very similar results with respect to the average streamflow, standard deviation and the N-S efficiency. The LS-SVM-R and the MLR techniques reproduced the observed average streamflow in the calibration phase

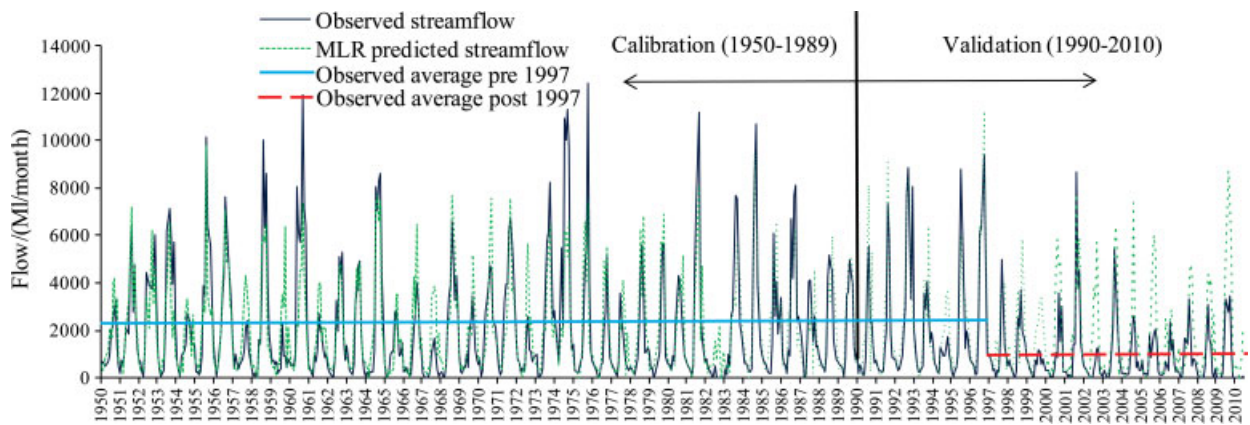


Figure 6. Observed streamflow and MLR-predicted streamflow.

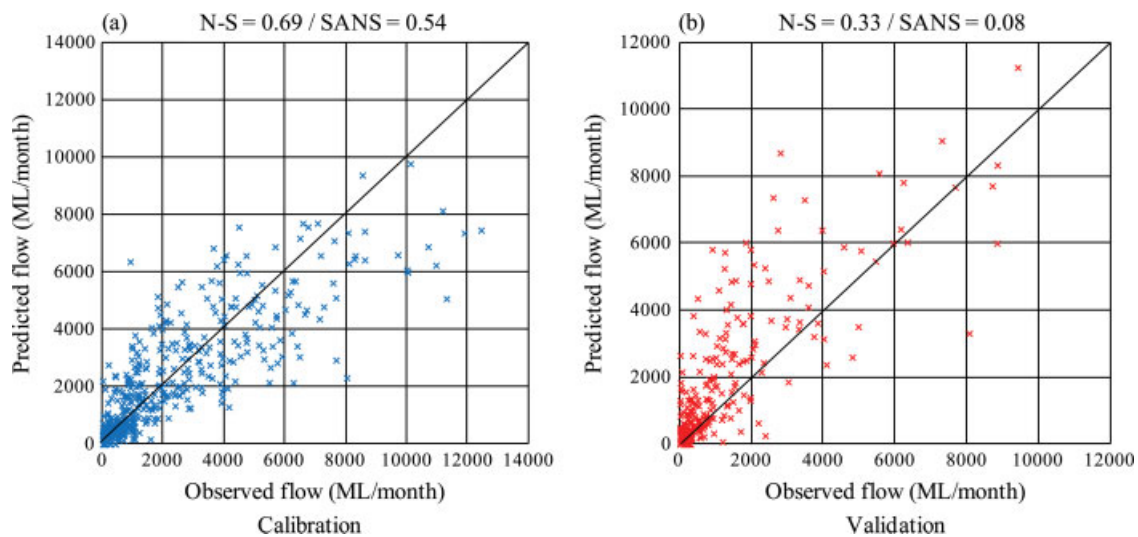


Figure 7. Scatter plots for calibration and validation phases of MLR-based model.

with a high degree of accuracy. The standard deviation was not reproduced in calibration with an equal level of precision by either of the two techniques. In validation, both modelling techniques over-estimated the overall average of streamflows as well as the standard deviation of the observations, but MLR over-estimated these statistics more than that of LS-SVM-R. The MLR modelling technique displayed relatively poor results in comparison to LS-SVM-R in validation in terms of N-S efficiency, though MLR could produce equally good predictions as LS-SVM-R in calibration. The coefficient of determination (R^2) also provided an evaluation of model performances, comparable to that of N-S efficiency, for the calibration and validation of the two models.

Table V provides the performance details of the LS-SVM-R and MLR modelling techniques on a seasonal basis. For all the four seasons, during calibration, the LS-SVM-R and MLR modelling techniques reproduced the observed average streamflow successfully, but neither of the two could correctly capture the observed standard deviation and coefficient of variation of the streamflow. In validation, LS-SVM-R- and MLR-based models

clearly over-estimated the monthly averages of streamflows for all the four seasons. In summer, the MLR-based model yielded better performances than the LS-SVM-R-based model displaying higher N-S efficiencies, during both calibration and validation. The worst validation results were produced by the MLR-based model in autumn with an N-S efficiency of -3.70 ; during the same period, the LS-SVM-R-based model also failed with an N-S efficiency of -2.45 . Both modelling techniques displayed overall SANS efficiencies quite comparable with the N-S efficiencies for the four seasons, in calibration and validation. It was observed that the original N-S formula produces overall model efficiencies higher than the model efficiencies of seasons when there is a strong seasonality in the streamflow regime.

4.9. Results of PC-based LS-SVM-R downscaling model calibration and validation

The PC-based LS-SVM-R models developed for January exhibited much poor performances in comparison with the non-PC models (i.e. the models developed with the

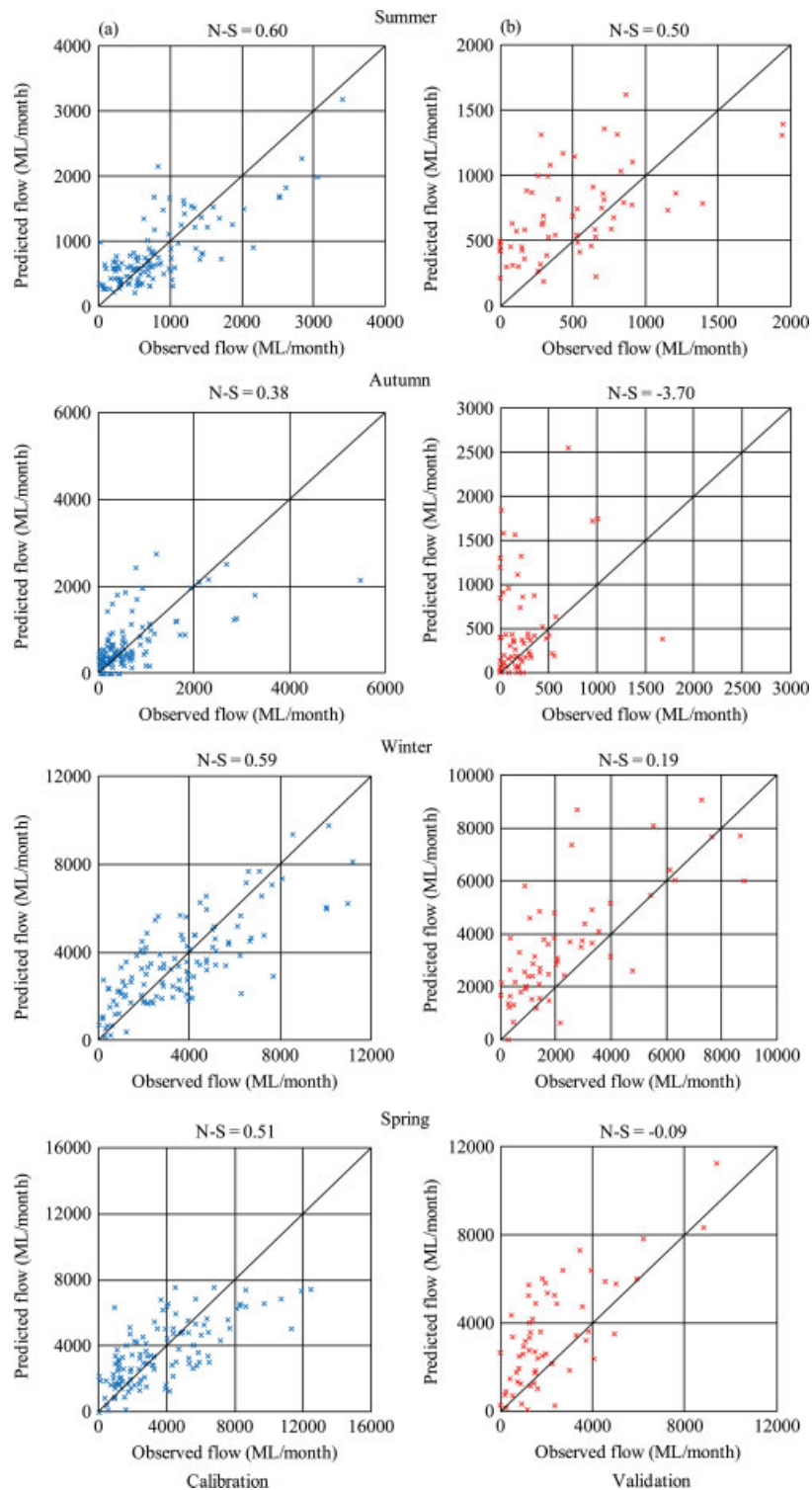


Figure 8. Seasonal scatter plots for calibration (left) and validation (right) of MLR-based model.

original standardized variables). Table VI shows a comparison of performances of non-PC and PC models developed using the LS-SVM-R technique for January. The performances were measured with the N-S efficiency. It was clearly observed that the non-PC model produces much better results than the PC-based models in validation. In calibration, the PC models suffered severe overfitting as seen by poor performances during validation,

though they displayed increasingly high N-S efficiencies during calibration with the number of PCs introduced to it.

The PC-based LS-SVM-R models developed for December displayed comparatively good results with the non-PC model. Table VII provides a comparison of performances of the non-PC model with the PC-based models, established with LS-SVM-R for December.

Table IV. Overall performances of LS-SVM-R and MLR modelling approaches.

Statistic	Calibration (1950–1989)			Validation (1990–2010)		
	Observation	SVM	MLR	Observation	SVM	MLR
Avg	2129.33	2130.00	2132.00	1318.55	1910.00	2018.00
Std	2387.32	1975.15	1984.92	1788.14	1917.13	2124.94
C_v	1.12	0.93	0.93	1.36	1.00	1.05
SANS		0.59	0.54		0.27	0.08
N-S		0.73	0.69		0.47	0.33
R^2		0.73	0.69		0.65	0.63

Avg = average monthly streamflow in ML month⁻¹; Std = standard deviation of the streamflow in ML month⁻¹; C_v = coefficient of variation; SANS = seasonally adjusted Nash–Sutcliffe efficiency; N-S = Nash–Sutcliffe efficiency; R^2 = coefficient of determination.

Table V. Season-wise performances of LS-SVM-R and MLR modelling approaches.

Model	Statistic	Calibration Season				Validation Season			
		Summer	Autumn	Winter	Spring	Summer	Autumn	Winter	Spring
Observed	Avg	794.69	676.69	3530.21	3515.74	612.43	232.98	2322.14	2167.73
LS-SVM-R		794.69	680.25	3530.21	3515.81	828.73	496.45	3299.94	3097.70
MLR		794.69	683.37	3530.21	3521.28	744.47	505.61	3501.36	3414.12
Observed	Std	648.73	1028.03	2501.21	2713.95	1047.29	284.99	2152.02	1947.18
LS-SVM-R		431.22	630.80	1814.37	1999.07	420.69	517.84	1788.23	2179.77
MLR		504.26	626.49	1921.14	1919.39	468.94	554.83	2094.47	2309.65
Observed	C_v	0.81	1.52	0.71	0.77	1.71	1.22	0.93	0.90
LS-SVM-R		0.54	0.93	0.51	0.57	0.51	1.04	0.54	0.70
MLR		0.63	0.92	0.54	0.55	0.63	1.10	0.60	0.68
LS-SVM-R	N-S	0.55	0.45	0.56	0.62	0.39	-2.45	0.38	0.16
MLR		0.60	0.38	0.59	0.50	0.50	-3.70	0.19	-0.09
LS-SVM-R	R^2	0.56	0.46	0.56	0.63	0.55	0.22	0.60	0.54
MLR		0.60	0.38	0.59	0.51	0.65	0.07	0.55	0.53

Avg = average monthly streamflow in ML month⁻¹; Std = standard deviation of the streamflow in ML month⁻¹; C_v = coefficient of variation; N-S = Nash–Sutcliffe efficiency; R^2 = coefficient of determination.

Table VI. Performances of non-PC model against the PC-based models for January.

Month	Phase	Non-PC Model 8 inputs	5 PCs, 98% variance explained	6 PCs, 99.4% variance explained	7 PCs, 99.7% variance explained	8 PCs, 100% variance explained
January	Calibration	0.37	0.55	0.77	0.80	0.93
	Validation	0.16	-0.07	-0.17	-0.18	-0.78

Table VII. Performances of non-PC model against the PC-based models for December.

Month	Phase	Non-PCs Model 10 inputs	7 PCs, 98.3% variance explained	8 PCs, 99.1% variance explained	9 PCs, 99.8% variance explained	10 PCs, 100% variance explained
December	Calibration	0.40	0.37	0.37	0.40	0.38
	Validation	0.37	0.30	0.32	0.26	0.30

When the number of PCs was increased from seven to ten, the model performances in calibration and validation showed only a slight fluctuation and remained mainly static.

According to the results given in Tables VI and VII, it was seen that the models based on PCs performed well for December, failed for January, in comparison with the corresponding non-PC models. This was an interesting

finding, as in general a PC-based model should perform equally well as its non-PC model, since PCs are linear combinations of the original variables from which they were extracted.

5. Discussion

This study incorporated the volumetric soil moisture content in the 0- to 10- and 10- to 200-cm soil layer, which have not been used as probable predictors in past streamflow downscaling studies. The selection of soil moisture was based on the fact that it is highly influential on the generation of streamflows (Timbal *et al.*, 2002). Soil retains moisture received from rain and depending on its moisture content at the time, can reduce the wetting up required before runoff is generated. Stored water can also be subsequently released into streams, acting as a temporary storage reservoir. This action lags the influences of the rainfall on the streamflow generation, highlighting the importance of the role played by soil moisture on streamflow generation. For February, May, June and October, model inputs were dominated by the two soil moisture parameters, due to the reasonably good correlations (0.40–0.65) observed between the soil moisture and streamflow during these months.

The potential predictor selection was performed with the Pearson correlation coefficients between the predictors and the streamflows under three 20-year time slices, unlike in past studies, where a single correlation over the entire period of study has been considered. In this study, the use of three 20-year time slices allowed the extraction of the best correlated variables consistently over time from the set of probable predictors concerned. The predictors that showed good correlations consistently over the three time slices with the streamflows were more likely to maintain similar correlation under changing climate in future. In other words, predictors that showed correlations with less fluctuation in terms of magnitudes and signs, over time, are more likely to have consistent relationships with streamflows in the future than the predictors that did not exhibit the above characteristics. Therefore, the use of multiple correlations under several time slices will aid in the selection of more reliable potential variables leading to a more reliable downscaling model. However, there is no guarantee of the nature of the correlation that the predictors will have in the future, with streamflows.

LS-SVM-R and MLR techniques exhibited equally good overall performances in calibration, but in validation, LS-SVM-R performed better than MLR. Both modelling techniques under-estimated the majority of high flows in calibration, and in validation, an over-estimating trend of the majority of flows was observed. The level of uncertainty associated with very high and very low observed streamflows should be noted as it is within this data range that most uncertainty is introduced during streamflow measurements and with the associated rating curve. In general, due to practical difficulties, rating

curves are developed with the streamflow data corresponding to ordinary flow conditions of a river. This leads to extrapolation of the rating curve for high flows leading to errors in the estimation of high streamflows (Di Baldassarre and Montanari, 2009). When the downscaling models are calibrated to these data containing less reliable low/high flows, it could possibly lead to errors in the model, producing erroneous streamflow predictions. This could be one source of errors in streamflows data, used in this study, which has possibly contributed to errors in the predictions of flows by the LS-SVM and MLR downscaling models. Summer and winter flow conditions were better predicted than those of autumn and spring by LS-SVM-R and MLR techniques. The worst flow predictions were seen in the autumn validation. The limited prediction ability of the LS-SVM-R and MLR downscaling models in autumn well agreed with the findings of Robertson and Wang (2008), where a Bayesian joint probability model was used to predict seasonal streamflows over Victoria. The model failure in autumn could be due to the fact that, before autumn the Victorian catchments are generally at a dry condition, and when the catchments get wet in autumn, they absorb most of the rain water depending on different antecedent soil moisture conditions and this causes the autumn rainfall to produce irregular contributions to the streamflows. However, this phenomenon needs more scientific investigation but has been believed to be true in Victorian catchments.

The use of SANS efficiency is recommended in studies where the averages of streamflows in different seasons are significantly different from the overall average of the streamflow. The SANS efficiency estimates the model performances considering the seasonal averages of the streamflows, whereas the original N-S formula uses the overall average of streamflows across all seasons. When applied to a streamflow data set exhibiting strong seasonality, the original N-S formula produces higher overall model efficiency than those for the four seasons. Owing to the inclusion of seasonal averages of streamflows, SANS efficiency produces overall model performances comparable to those for the four seasons. It is advisable to use N-S and SANS efficiencies in addition to graphical techniques of model evaluation such as scatter and time series plots to calibrate and validate the downscaling models. Graphical illustrations of the results of a model could provide an overall picture of the model predictions against observations, but a numerical performance criterion could only produce only a numerical value to reflect model performances.

Particularly after 1997, LS-SVM-R- and MLR-based downscaling models tended to largely over-estimate the high streamflows. The failure to correctly predict the high values of the predictands such as streamflows and rainfalls was a well-observed phenomenon in many of the past downscaling exercises (e.g. Ghosh and Mujumdar, 2008). This is mainly because statistical downscaling models fail to capture the entire

variance of the predictands (Tripathi *et al.*, 2006). The time series plots of the 23 NCEP/NCAR probable predictors averaged over the atmospheric domain did not show any clear climate change signal corresponding to the post-1997 period, where a clear step down in the observed streamflow time series was seen.

In downscaling GCM outputs to streamflows, it is highly advisable to expose the statistical downscaling model to the widest possible range (from very low flows to extremely high flows) of the observed streamflows. This allows the statistical downscaling model to be fine-tuned to the whole range of streamflows, resulting in better performances in validation and more reliable future flow projections. In this study, the calibration period (1950–1989) contained a wide range of flows (ranging from 0 to 12 427 ML month⁻¹), though it contained more high flows in comparison to the validation period. In the validation period (1990–2010), the observed streamflow ranged between 0 and 9387 ML month⁻¹. According to the above-mentioned facts and the time series plot of observed streamflows (Figure 3), it was clear that although there were no intense droughts in the calibration period, it included a wide range of flows adequate for the satisfactory calibration of the model. Therefore, it was suspected that the limited performances of the LS-SVM and MLR models in validation period would possibly be more associated with the NCEP/NCAR predictors, which did not show a clear climate change signal corresponding to the severe drought observed during the validation. It was found that even when the downscaling model is calibrated for the period 1990–2010 (which is the original validation period), the model failed to adequately reproduce the magnitudes of observed streamflows (over-estimation of observed high flows etc.), although the seasonal pattern was correctly modelled, during the severe drought that occurred after 1997. This reinforced the conclusion that the limited performances of the LS-SVM and MLR statistical downscaling models in the validation period (1990–2010) was clearly due to the failure of NCEP/NCAR predictors, in properly characterizing the drought during the post-1997 period. Therefore, it was understood that when the inputs to the downscaling model do not correctly characterize the regional climate, even if the calibration and validation periods are changed, the model performances are hardly expected to improve.

The post-1997 drought in Victoria is regarded as the most severe drought (at times referred to as the Millennium drought) observed in the historic records. Although the GCM outputs used in this study did not exhibit a clear climate change signal corresponding to this severe drought, both LS-SVM- and MLR-based downscaling models have correctly captured the seasonal pattern of the streamflow (Figures 3 and 6) throughout the study period, despite the fact that the models have failed to reproduce the magnitudes of streamflows adequately. Therefore, in this study, the outputs of the two statistical downscaling models (LS-SVM and MLR) have proven that

even during an hydroclimatic extreme such as the Millennium drought mentioned here, at least the seasonal pattern of the actual streamflow could be correctly predicted with the GCM outputs. The seasonal pattern of the streamflows could still aid in the water resources planning and management by providing a hint of the future streamflow trends. According to Zhang *et al.* (2010), the knowledge of trends in the streamflow is important for the efficient management of water resources. Furthermore, the post-1997 drought in Victoria was a rare extreme hydroclimatic event, and therefore, model failures such as that seen here are unlikely to be frequent.

El Niño southern oscillation index (SOI), southern annular mode and sea surface temperature (SST) indices, including NINO 3, NINO 4, NINO 3.4, Indian Ocean dipole and Indonesian SST index are reported to be some of the climate indices that are influential on the climate of Australia (Langford *et al.*, 2011). In this study, the lag zero and other lagged correlations between the streamflow and SOI and NINO 3.4 indices were computed. With streamflows, SOI and NINO 3.4 displayed increasingly poor correlations with the increase in lag, indicating the absence of a clear climate change signal in these indices, corresponding to the recent Victorian drought started in 1997. Though some of these indices showed poor correlations with streamflows, still these could aid in the process of identifying an onset of a wet or a dry hydroclimatic regime to occur. This will enable the development and use of two different downscaling models, one fine tuned for a relatively wet regime and the other fine tuned for a relatively dry regime, leading to more accurate predictions. Further studies will be performed to analyse the influence of the above-mentioned climate indices on the streamflow over this study area, aiming to improve the performances of the downscaling models already developed in this study.

The performances of the PC-based LS-SVM-R models revealed that the PC analysis should be used with caution in preparing input variables for a downscaling model. In this study, the coefficients of PCs derived for the calibration phase (based on the calibration predictor data) were applied on the validation predictor data to generate PCs for the validation phase. These coefficients of PCs are needed for generating PC inputs for the downscaling model for future hydroclimatic projections, since they become a static component of the model. This process could distort the PCs in validation by making them markedly correlated, which was a violation of the near-zero correlation property of PCs. Theoretically, PCs should display zero or near-zero correlations among each other. The PCs corresponding to the calibration phase remained zero or near-zero correlated. The PCs derived for the validation of the January LS-SVM-R models were more correlated among each other than those of December, possibly causing a greater failure for January model during the validation.

6. Conclusions

This study provides a detailed comparison of the use of least square support vector machine regression (LS-SVM-R) and multi-linear regression (MLR) for downscaling monthly general circulation model (GCM) outputs to catchment-level monthly streamflows. Downscaling streamflows directly from the GCMs minimizes the time and effort involved in complex hydrologic modelling, in predicting streamflows. To the best of the authors' knowledge, this article presents the first effort in statistically downscaling GCM outputs directly to catchment streamflows in Australia.

The inclusion of soil moisture parameters in probable GCM predictors enabled the consideration of contribution of soil moisture in streamflow generation. The study emphasized the selection of consistently correlated GCM predictors with the predictand, over the entire period of the analysis, since this allows for the building a more robust downscaling model. This was performed by splitting the entire predictor (GCM outputs)–predictand (streamflow) data set into three 20-year time slices and selecting the predictors that showed good, statistically significant Pearson correlation coefficients with the predictand consistently over all the three time slices and during the whole period.

Based on the results of the present downscaling study, it was concluded that LS-SVM-R has a better potential in downscaling GCM predictors to catchment-level streamflows than that of MLR, but still MLR is a potential technique for a statistical downscaling study. The LS-SVM-R- and MLR-based downscaling models developed in this study showed reasonable capability in predicting the streamflows in summer and winter despite the limited performances shown in autumn. The low performances in the downscaling models after the 1997 drought in Victoria was clearly due to the absence of a clear climate change signal in the GCM predictors used in the study. This was proven by the limited performances exhibited by the LS-SVM model, when it was calibrated for the 1990–2010 period, which included the post-1997 drought. However, a robust downscaling model should be able to produce reasonable predictions in validation irrespective of the hydroclimatic regime to which it was exposed in the calibration.

Acknowledgements

The authors acknowledge the financial assistance provided by the Australian Research Council Linkage Grant LP 100100554 and the useful thoughts of Dr Daniel Lai at the Victoria University. The authors also wish to thank the editor and the two anonymous reviewers for their useful comments, which have improved the quality of this article.

References

Anandhi A, Srinivas VV, Kumar DN, Nanjundiah RS. 2009. Role of predictors in downscaling surface temperature to river

basin in India for IPCC SRES scenarios using support vector machine. *International Journal of Climatology* **29**: 583–603, DOI: 10.1002/joc.1719.

Anandhi A, Srinivas VV, Nanjundiah RS, Kumar DN. 2008. Downscaling precipitation to river basin in India for IPCC SRES scenarios using support vector machine. *International Journal of Climatology* **28**: 401–420, DOI: 10.1002/joc.1529.

Basak D, Pal S, Patranabis DC. 2007. Support vector regression. *Neural Information Processing-Letters and Reviews* **11**: 203–224.

Benestad RE, Hanssen-Bauer I, Førland EJ. 2007. An evaluation of statistical models for downscaling precipitation and their ability to capture long-term trends. *International Journal of Climatology* **27**: 649–665, DOI: 10.1002/joc.1421.

Cannon AJ, Whitfield PH. 2002. Downscaling recent streamflow conditions in British Columbia, Canada using ensemble neural network models. *Journal of Hydrology* **259**: 136–151, DOI: 10.1016/S0022-1694(01)00581-9.

Cayley RA, Taylor DH. 1997. Grampians special map area and geological report. Geological Survey of Victoria Report 107, 42–130.

Chen TS, Yu PS, Tang YH. 2010. Statistical downscaling of daily precipitation using support vector machines and multivariate analysis. *Journal of Hydrology* **385**: 13–22, DOI: 10.1016/j.jhydrol.2010.01.021.

Cheng CS, Li G, Li Q, Auld H. 2008. Statistical downscaling of hourly and daily climate scenarios for various meteorological variables in south-central Canada. *Theoretical and Applied Climatology* **91**: 129–147, DOI: 10.1007/s00704-007-0302-8.

Chiew FHS, Young WJ, Cai W, Teng J. 2010. Current drought and future hydroclimate projections in southeast Australia and implications for water resources management. *Stochastic Environmental Research and Risk Assessment* **25**: 602–612, DOI: 10.1007/s00477-010-0424-x.

Chu JT, Xia J, Xu CY, Singh VP. 2010. Statistical downscaling of daily mean temperature, pan evaporation and precipitation for climate change scenarios in Haihe River, China. *Theoretical and Applied Climatology* **99**: 149–161, DOI: 10.1007/s00704-009-0129-6.

Cosma S, Richard E, Miniscloux F. 2002. The role of small-scale orographic features in the spatial distribution of precipitation. *Quarterly Journal of the Royal Meteorological Society* **128**: 75–92, DOI: 10.1256/00359000260498798.

De Brabanter K, Karsmakers P, Ojeda F, Alzate C, De Brabanter J, Pelckmans K, De Moor B, Vandewalle J, Suykens JAK. 2010. LS-SVMlab toolbox user's guide. Internal Report 10–146. K.U. Leuven University: Belgium, 25–27.

Di Baldassarre G, Montanari A. 2009. Uncertainty in river discharge observations: a quantitative analysis. *Hydrology and Earth System Sciences Discussions* **6**: 39–61, DOI: 10.5194/hessd-6-39-2009.

Drucker H, Burges CJC, Kaufman L, Smola A, Vapnik V. 1996. Support vector regression machines. *Advances in Neural Information Processing Systems* **9**: 155–161.

Enke W, Spegat A. 1997. Downscaling climate model outputs into local and regional weather elements by classification and regression. *Journal of Climate Research* **8**: 195–207, DOI: 10.3354/cr0008195.

Fowler HJ, Blenkinsop S, Tebaldi C. 2007. Linking climate change modelling to impacts studies: recent advances in downscaling techniques for hydrological modelling. *International Journal of Climatology* **27**: 1547–1578, DOI: 10.1002/joc.1556.

Ghosh S, Mujumdar PP. 2008. Statistical downscaling of GCM simulations to streamflow using relevance vector machine. *Advances in Water Resources* **31**: 132–146, DOI: 10.1016/j.advwatres.2007.07.005.

Giorgi F, Hewitson B, Christensen J, Hulme M, Von Storch H, Whetton P, Jones R, Mearns L, Fu C. 2001. Climate change 2001, The scientific basis, contribution of working group I to the third assessment report of the IPCC, Chapter 10, 583–638. Available at <http://www.grida.no/> (Accessed 7 November 2011).

GWMWater. 2011. Storage management rules for the Wimmera Mallee system headworks, 5–6. Available at http://www.gwmwater.org.au/information/publications/ground-and-surface-water/west-wimmera-gma/cat_view/163-reservoir-operating-rules (Accessed 1 March 2012).

Helsel DR, Hirsch RM. 2002. *Statistical Methods in Water Resources Techniques of Water Resources Investigations*, Book 4, Chapter A3. U.S. Geological Survey, 295–297 Available at http://pubs.usgs.gov/twri/twri4a3/html/pdf_new.html (Accessed 10 October 2011).

Heyen H, Zorita E, von Storch, H. 1996. Statistical downscaling of monthly mean North Atlantic air-pressure to sea level anomalies

- in the Baltic Sea. *Tellus* **48**: 312–323, DOI: 10.1034/j.1600-0870.1996.t01-1-00008.x.
- Hughes L. 2000. Biological consequences of global warming: is the signal already apparent. *Trends in Ecology and Evolution* **15**: 56–61, DOI: 10.1111/j.1749-4877.2010.00200.x.
- Hughes L. 2003. Climate change and Australia: trends, projections and impacts. *Austral Ecology* **28**: 423–443, DOI: 10.1046/j.1442-9993.2003.01300.x.
- Huth R. 2002. Statistical downscaling of daily temperature in central Europe. *Journal of Climate* **15**: 1731–1742, DOI: 10.1175/1520-0442(2002)015.
- Huth R. 2005. Downscaling of humidity variables: a search for suitable predictors and predictands. *International Journal of Climatology* **25**: 243–250, DOI: 10.1002/joc.1122.
- Kalnay E, Kanamitsu M, Kistler R, Collins W, Deaven D, Gandin L, Iredell M, Saha S, White G, Woollen J, Zhu Y, Chelliah M, Ebisuzaki W, Higgins W, Janowiak J, Mo KC, Ropelewski C, Wang J, Leetmaa A, Reynolds R, Jenne R, Joseph D. 1996. The NCEP/NCAR reanalysis project. *Bulletin of the American Meteorological Society* **77**: 437–471, DOI: 10.1175/1520-0477(1996)077<0437:TNYRP>2.0.CO;2.
- Karl TR, Wang WC, Schlesinger ME, Knight RW, Portman D. 1990. A method of relating general circulation model simulated climate to the observed local climate Part I: seasonal statistics. *Journal of Climate* **3**: 1053–1079, DOI: 10.1175/1520-0442(1990)003<1053:AMORGC>2.0.CO;2.
- Landman WA, Mason SJ, Tyson PD, Tennant WJ. 2001. Statistical downscaling of GCM simulations to streamflow. *Journal of Hydrology* **252**: 221–236, DOI: 10.1016/S0022-1694(01)00457-7.
- Langford SV, Hendon HH, Lim EP. 2011. Assessment of POAMA's predictions of some climate indices for use as predictors of Australian rainfall. CAWCR Technical Report No. 31, 3–4.
- Maurer EP, Hidalgo HG. 2008. Utility of daily vs. monthly large-scale climate data: an intercomparison of two statistical downscaling methods. *Hydrology and Earth System Science* **12**: 551–563, DOI: 10.5194/hess-12-551-2008.
- Murphy J. 1998. An evaluation of statistical and dynamical techniques for downscaling local climate. *International Journal of Climate* **12**: 2256–2284, DOI: 10.1175/1520-0442(1999)012<2256:AEOSAD>2.0.CO;2.
- Muzik I. 2002. A first-order analysis of the climate change effect on flood frequencies in a subalpine watershed by means of a hydrological rainfall–runoff model. *Journal of Hydrology* **267**: 65–73, DOI: 10.1016/S0022-1694(02)00140-3.
- Najafi M, Moradkhani H, Wherry S. 2011. Statistical downscaling of precipitation using machine learning with optimal predictor selection. *Journal of Hydrologic Engineering* **16**: 650–664, DOI: 10.1061/(ASCE)HE.1943-5584.0000355.
- Nash JE, Sutcliffe JV. 1970. River flow forecasting through conceptual models, part 1 – a discussion of principles. *Journal of Hydrology* **10**: 282–290, DOI: 10.1016/0022-1694(70)90255-6.
- Nelder JA, Mead R. 1965. A simplex method for function minimization. *The Computer Journal* **7**: 308–313, DOI: 10.1093/comjnl/7.4.308.
- Pearson K. 1895. Mathematical contributions to the theory of evolution. iii. Regression heredity and panmixia. *Philosophical Transactions of the Royal Society of London Series A* **187**: 253–318, DOI: 10.1098/rsta.1896.0007.
- Phillips ID, McGregor GR, Wilson CJ, Bower D, Hannah DM. 2003. Regional climate and atmospheric circulation controls on the discharge of two British rivers, 1974–97. *Theoretical and Applied Climatology* **76**: 141–164, DOI: 10.1007/s00704-003-0021-8.
- Robertson DE, Wang QJ. 2008. An investigation into the selection of predictors and skill assessment using the Bayesian joint probability (BJP) modelling approach to seasonal forecasting of streamflows. CSIRO Water for a healthy country flagship report, 14.
- Root T, Price J, Hall K, Schneider S, Rosenzweig C, Pounds J. 2003. Fingerprints of global warming on wild animals and plants. *Nature* **421**: 57–60, DOI: 10.1038/nature01333.
- Ruiz JE, Cordery I, Sharma A. 2007. Forecasting streamflows in Australia using the tropical Indo-Pacific thermocline as predictor. *Journal of Hydrology* **341**: 156–164, DOI: 10.1016/j.jhydrol.2007.04.021.
- Salameh T, Drobinski P, Vrac M, Naveau P. 2009. Statistical downscaling of near-surface wind over complex terrain in southern France. *Journal of Meteorology and Atmospheric physics* **103**: 253–265, DOI: 10.1007/s00703-008-0330-7.
- Sinclair KM. 2004. Wimmera-Malle simulation model – annual update methodology. A report by Sinclair Knight Merz, Melbourne, Australia, 21–79.
- Smith I, Chandler E. 2009. Refining rainfall projections for the Murray Darling basin of south-east Australia – the effect of sampling model results based on performance. *Journal of Climate Change* **102**: 377–393, DOI: 10.1007/s10584-009-9757-1.
- von Storch H, Zorita E, Cubasch U. 1993. Downscaling of global climate change estimates to regional scales: an application to Iberian rainfall in wintertime. *Journal of Climate* **6**: 1161–1171, DOI: 10.1175/1520-0442(1993)006<1161:DOGCC>2.0.CO;2.
- Sullivan CA, Huntingford C. 2009. Water resources, climate change and human vulnerability. In *Proceedings of the 18th World IMACS/MODSIM Congress*. 13–17 July 2009. Cairns, Australia, 3984–3990.
- Suykens JAK, Vandewalle J. 1999. Least squares support vector machine classifiers. *Neural Information Processing – Letters and Reviews* **9**: 293–300, DOI: 10.1023/A:1018628609742.
- Suykens JAK, Van Gestel T, De Brabanter J, De Moor B, Vandewalle J. 2002. *Least Squares Support Vector Machines*. World Scientific: Singapore, 29–111.
- Timbal B, Fernandez E, Li Z. 2009. Generalization of a statistical downscaling model to provide local climate change projections for Australia. *Environmental Modeling and Software* **24**: 341–358, DOI: 10.1016/j.envsoft.2008.07.007.
- Timbal B, Power S, Colman R, Viviani J, Lirola S. 2002. Does soil moisture influence climate variability and predictability over Australia?. *Journal of Climate* **15**: 1230–1238, DOI: 10.1175/1520-0442(2002)015<1230:DSMICV>2.0.CO;2.
- Tisseuil C, Vrac M, Lek S, Wade AJ. 2010. Statistical downscaling of river flows. *Journal of Hydrology* **385**: 279–291, DOI: 10.1016/j.jhydrol.2010.02.030.
- Tripathi S, Srinivas VV, Nanjundiah RS. 2006. Downscaling of precipitation for climate change scenarios: a support vector machine approach. *Journal of Hydrology* **330**: 621–640, DOI: 10.1016/j.jhydrol.2006.04.030.
- Vapnik V. 2000. *The Nature of Statistical Learning Theory*. Springer-Verlag: New York, 17–298.
- Victorian Government Department of Sustainability and Environment. 2008. Climate Change in Victoria Summary Report, 7. Available at <http://www.climatechange.vic.gov.au/publications> (Accessed on 1 November 2011).
- Wang W. 2006. *Stochasticity, Nonlinearity and Forecasting of Streamflow Processes*. Deft University Press: Amsterdam, 72–73.
- Whitehead PG, Wilby RL, Battarbee RW, Kernan M Wade AJ. 2009. A review of the potential impacts of climate change on surface water quality. *Hydrological Sciences* **54**: 101–123, DOI: 10.1623/hysj.54.1.101.
- Wilby RL, Charles SP, Zorita E, Timbal B, Whetton P, Mearns LO. 2004. Guidelines for use of climate scenarios developed from statistical downscaling methods, supporting material to the IPCC, 3–21. Available at <http://www.ipcc-data.org/> (Accessed 1 November 2011).
- Wilby RL, Wigley TML. 1997. Downscaling general circulation model output: a review of methods and limitations. *Progress in Physical Geography* **21**: 530–548, DOI: 10.1177/030913339702100403.
- Wilby RL, Wigley TML. 2000. Precipitation predictors for downscaling: observed and general circulation model relationships. *International Journal of Climatology* **20**: 641–661, DOI: 10.1002/(SICI)1097-0088(200005).
- Wilks DS, Wilby RL. 1999. The weather generation game: a review of stochastic weather models. *Progress in Physical Geography* **23**: 329–357, DOI: 10.1177/030913339902300302.
- Xu C. 1999. From GCMs to river flow: a review of downscaling methods and hydrologic modeling approaches. *Progress in Physical Geography* **23**: 229–249, DOI: 10.1177/030913339902300204.
- Xu ZX, Zhao FF, Li JY. 2009. Response of streamflow to climate change in the headwater catchment of the Yellow River basin. *Quaternary International* **208**: 62–75, DOI: 10.1016/j.quaint.2008.09.001.
- Zhang Z, Dehoff AD, Pody RD. 2010. New approach to identify trend pattern of streamflows. *Journal of Hydrologic Engineering* **15**: 244–248, DOI: 10.1061/(ASCE)HE.1943-5584.0000179.
- Zhou J, Shi J, Li G. 2011. Fine tuning support vector machines for short-term wind speed forecasting. *Energy Conversion and Management* **52**: 1990–1998, DOI: 10.1016/j.enconman.2010.11.007.